



NJC

High-Spin Enforcement in First-Row Metal Complexes of a Constrained Polyaromatic Ligand: Synthesis, Structure, and Properties

Journal:	<i>New Journal of Chemistry</i>
Manuscript ID	NJ-ART-04-2018-002072.R1
Article Type:	Paper
Date Submitted by the Author:	13-Oct-2018
Complete List of Authors:	Chen, Lizhu; University of Mississippi, Chemistry and Biochemistry Dulaney, Hunter; University of Mississippi, Chemistry and Biochemistry Wilkins, Branford; Texas A&M University, Chemistry Farmer, Sarah; University of Mississippi, Chemistry and Biochemistry Zhang, Yanbing; University of Mississippi, Chemistry Fronczek, Frank; Louisiana State University, Chemistry Dept Jurss, Jonah; University of Mississippi, Chemistry and Biochemistry

SCHOLARONE™
Manuscripts

High-Spin Enforcement in First-Row Metal Complexes of a Constrained Polyaromatic Ligand: Synthesis, Structure, and Properties

Lizhu Chen,¹ Hunter A. Dulaney,¹ Branford O. Wilkins,² Sarah Farmer,¹ Yanbing Zhang,¹ Frank R. Fronczek,³ Jonah W. Jurss^{1*}

¹Department of Chemistry and Biochemistry, University of Mississippi, University, MS 38677, USA.

²Department of Chemistry, Texas A&M University, College Station, TX 77843, USA.

³Department of Chemistry, Louisiana State University, Baton Rouge, LA 70803, USA.

Abstract

The coordination chemistry of a rigid tetradentate polypyridyl ligand has been developed with first-row transition metals Mn(II), Fe(II), Co(II), Ni(II), and Zn(II). The polyaromatic ligand, 2,2'-di([2,2'-bipyridin]-6-yl)-1,1'-biphenyl (**5**, bpbb), is comprised of 2,2'-bipyridine donors positioned at the 2 and 2' carbons of a biphenyl backbone. Notably, coordination of the typical strong field bipyridine fragments is constrained, weakening the octahedral ligand fields around manganese, iron, and cobalt to give high-spin electronic states. Solution magnetic susceptibility measurements were conducted across the series using the Evans method and variable-temperature solid-state SQUID magnetometry was performed on two Fe(II) compounds, including a bis(thiocyanato) species. Spin crossover behavior was not observed as the compounds remained high-spin over the entire temperature range. The impact of the biphenyl bridge on M-N bond distances and redox potentials has also been assessed by comparison to relevant first-row metal bis- and tris-bipyridine compounds from the literature.

Introduction

Tetradentate and pentadentate ligand frameworks are important classes of ligands for accessing stable first-row transition metal complexes. The metal-ligand bonds of 3d metals are often labile and prone to substitution. Thus, highly chelating ligands are frequently employed to counter this characteristic while affording well-defined coordination spheres with tunable properties. Given the high denticity of these ligand classes, the number and relative orientation of labile coordination sites can be controlled, and specific geometries enforced, by clever ligand design in which preorganization, rigidity, and steric factors are useful strategies.^{1,2}

Biphenyl-based polydentate ligands have been employed in a number of areas, including bioinorganic model compounds,²⁻⁴ spin crossover complexes,⁵ and homogeneous catalysis.⁶ These systems exploit biphenyl as an unyielding structural unit whose substituted phenyl groups are not coplanar, allowing the appended donors to bind at a single metal center but with limited flexibility. Octahedral Fe(II) compounds of general form $[\text{FeL}_6]^{2+}$ or $\text{FeL}_4(\text{NCS})_2$ (where L is an N-heterocyclic donor such as pyridine) comprise the vast majority of known spin crossover (SCO) compounds, which hold great promise for applications such as data storage and molecular electronics.⁷⁻⁹ SCO compounds are typically studied in the solid state where abrupt transitions between spin states can be observed.⁷⁻⁹ One strategy used to engender SCO behavior is the design of sterically demanding ligands that allow tuning of the metal-ligand bonding interactions to access complexes in which the ligand field strength and the spin-pairing energy are comparable.^{10,11} This commonly manifests through added substituents at positions adjacent to the donor atoms (i.e. the 6 and 6' positions of 2,2'-bipyridine or the 2 and 9 positions of 1,10-phenanthroline).^{12,13}

1
2
3
4 In this context, we sought to introduce strain remotely using a rigid polydentate scaffold as
5 an underexplored approach to SCO compounds. Our laboratory has been interested in
6 preorganized frameworks,¹⁴ as in the present case which involves a tetradentate ligand that
7 maximizes the chelate effect while dictating the metal coordination geometry through limited
8 rotation about single bonds connecting rigid donor moieties. Herein we report a straightforward
9 and improved synthesis of polyaromatic ligand 2,2'-di([2,2'-bipyridin]-6-yl)-1,1'-biphenyl² and
10 its metalation with mid-to-late first-row transition metals. Metal complexes of Mn(II), Fe(II),
11 Co(II), Ni(II), and Zn(II) were prepared to evaluate how the structural constraints of the ligand
12 are balanced with the geometric and electronic preferences of the metal centers. Solid-state
13 structures and optical, magnetic, and electrochemical properties of this series are described.
14
15

16 Experimental Section

17 **Materials and Methods.** Unless otherwise noted, all synthetic manipulations were carried
18 out using standard Schlenk techniques or in an MBraun glovebox under nitrogen atmosphere.
19 Tetrahydrofuran, dichloromethane, toluene, and diethyl ether were dried with a Pure Process
20 Technology solvent purification system. Compounds iodomethane, phosphorus(V) oxybromide,
21 2-tri-*n*-butylstannylpyridine, chlorobenzene, palladium(0) tetrakis(triphenylphosphine), and
22 dichloro(*p*-cymene)ruthenium(II) dimer were purchased from Oakwood Chemicals. Anhydrous
23 metal salts, iron(II) trifluoromethanesulfonate and iron(III) chloride, were purchased from Strem
24 Chemicals and Fisher Scientific, respectively. Potassium hexacyanoferrate(III) was purchased
25 from Sigma Aldrich and 2-phenylpyridine was acquired from Chem-Impex International. Water
26 was purified with a Barnstead NANOpure Diamond system. All other chemicals were reagent or
27 ACS grade, purchased from commercial vendors, and used without further purification. ¹H and
28 ¹³C NMR spectra were obtained using Bruker spectrometers operating at 300 or 500 MHz (¹H)
29 or 100 or 125 MHz (¹³C) as noted. Spectra were calibrated to residual protiated solvent peaks;
30 chemical shifts are reported in ppm. High-resolution electrospray ionization mass spectra (HR-
31 ESI-MS) were obtained with a Waters SYNAPT HDMS Q-TOF mass spectrometer and
32 elemental analyses of carbon, hydrogen, and nitrogen were conducted by Atlantic Microlab, Inc.,
33 Norcross, Georgia. UV-Vis spectra were recorded on an Agilent / Hewlett-Packard 8453 UV-
34 Visible Spectrophotometer with diode-array detector. Solution magnetic susceptibilities were
35 determined by NMR using the Evans method.¹⁵

36 **Electrochemical Measurements.** Electrochemistry was performed with a Bioanalytical
37 Systems, Inc. (BASi) Epsilon potentiostat employing a three-electrode cell equipped with glassy
38 carbon disk (3 mm dia.) working electrode, platinum wire counter electrode, and a silver wire
39 quasi-reference electrode. Cyclic voltammograms were collected in anhydrous acetonitrile
40 containing 0.1 M Bu₄NPF₆ electrolyte, and referenced at the end of experiments using ferrocene
41 as an internal standard.

42 **X-ray Crystallography.** Single crystals were coated with Paratone-N hydrocarbon oil and
43 mounted on the tip of a MiTeGen micromount. Temperature was maintained at 100 K with an
44 Oxford Cryostream 700 during data collection at the University of Mississippi, Department of
45 Chemistry and Biochemistry, X-ray Crystallography Facility. Samples were irradiated with Mo-
46 K α radiation with $\lambda = 0.71073$ Å using a Bruker Smart APEX II diffractometer equipped with a
47 Microfocus Sealed Source (Incoatec I μ S) and APEX-II detector. The Bruker APEX2 v. 2009.1
48 software package was used to integrate raw data which were corrected for Lorentz and
49 polarization effects.¹⁶ A semi-empirical absorption correction (SADABS) was applied.¹⁷ Space
50 groups were identified based on systematic absences, E-statistics, and successive refinement of
51
52
53
54
55
56
57
58
59
60

1
2
3 the structures. The structures were solved using direct methods and refined by least-squares
4 refinement on F^2 and standard difference Fourier techniques using SHELXL.¹⁸ Thermal
5 parameters for all non-hydrogen atoms were refined anisotropically, and hydrogen atoms were
6 included at ideal positions. For the structure of **5-Zn**, a poorly resolved outersphere diethyl ether
7 molecule could not be successfully modeled in the difference map. The data was treated with the
8 SQUEEZE procedure in PLATON.¹⁹ Full details of the structure determination in CIF format
9 have been deposited into The Cambridge Crystallographic Data Centre (CCDC), and have the
10 following deposition numbers: CCDC 1837621 (**5-Mn**), 1837622 (**5-Fe**), 1837623 (**5-Co**),
11 1837624 (**5-Ni**), and 1837625 (**5-Zn**). Coordination polyhedra for the central metal atoms were
12 produced using the Diamond 4.0 Crystal and Molecular Structure Visualization program.²⁰

13
14 **SQUID Magnetometry.** For both iron-containing compounds, crystals were crushed into a
15 polycrystalline powder and loaded into NORELL quartz NMR tubes. A slight excess by mass of
16 eicosane was deposited on top of the powder and the quartz tubes were flame sealed under
17 vacuum. The eicosane was melted in a warm water bath (42 °C) and allowed to re-solidify in
18 order to immobilize the powder samples. The sealed tubes were placed in straw sample holders,
19 and these sample holders were loaded into a Quantum Design MPMS 3 SQUID magnetometer
20 (TAMU Vice President of Research). DC (direct current) magnetic susceptibility measurements
21 of the samples were recorded under a static magnetic field of 0.1 T in the temperature range of
22 300 K to 2 K. The data was corrected for diamagnetic contributions from the straw and the
23 quartz tube. The intrinsic diamagnetism of the iron complexes and eicosane was also corrected
24 for by using Pascal's constants.¹⁵

25
26 **Synthesis.** A literature procedure was used for the preparation of 2,2'-di(pyridin-2-yl)-1,1'-
27 biphenyl, precursor **1**.²¹ A different synthetic route to ligand **5** (bpbb) has been reported
28 previously.²

29
30 *2,2'-([1,1'-biphenyl]-2,2'-diyl)bis(1-methylpyridin-1-ium) iodide, 2:* To a solution of **1** (0.50
31 g, 1.6 mmol) in acetonitrile (10 mL), iodomethane (1.5 mL, 24.1 mmol) was added dropwise
32 under nitrogen and the solution was refluxed for 2 days. A yellow suspension forms over the
33 course of the reaction. The reaction mixture is allowed to cool to room temperature before
34 diethyl ether (25 mL) is added and the precipitate is collected by vacuum filtration, washed with
35 diethyl ether, and dried to yield a light yellow solid (1.05 g, 60%). ¹H NMR (MeOD, 500 MHz):
36 δ 9.13 (d, $J = 6.3$ Hz, 2H), 8.41 (t, $J = 7.9$ Hz, 2H), 8.07 (t, $J = 1.6$ Hz, 2H), 7.8 (dd, $J = 8.0, 7.6$
37 Hz, 4H), 7.62 (t, $J = 7.6$, 2H), 7.56 – 7.49 (bt, 2H), 7.12 (s, 2H). ¹³C NMR (MeOD, 126 MHz): δ
38 148.878 (s), 146.75 (s), 138.81 (s), 133.60 (s), 133.03 (s), 132.56 (s), 132.17 (s), 131.84 (s),
39 130.86 (s), 130.35 (s), 128.82 (s), 128.37 (s). HR-ESI-MS (M^+) m/z calc. for [**2**]²⁺, 169.0891,
40 Found, 169.0901.

41
42 *6,6'-([1,1'-biphenyl]-2,2'-diyl)bis(1-methylpyridin-2(1H)-one), 3:* This reaction is performed
43 under air. $K_3Fe(CN)_6$ (2.48 g, 7.54 mmol) was dissolved in water (10.3 mL) and cooled to 0 °C.
44 Next, NaOH (2.51 g, 62.8 mmol) in water (9.4 mL) and **2** (0.93 g, 1.57 mmol) in water (4.7 mL)
45 were added dropwise to the first solution, simultaneously, *via* two dropping funnels over a period
46 of 1.5 h. The reaction mixture was then stirred for 3 h at 0 °C before it was heated at 40 °C
47 overnight. Saturated aqueous NaCl (28 mL) was added before dichloromethane (3 x 50 mL) was
48 used to extract the product. The organic phase was dried over anhydrous Na_2SO_4 and taken to
49 dryness by rotary evaporation. The resulting solid was dissolved in 8:2 ethyl acetate:methanol,
50 filtered through neutral alumina to remove impurities and taken to dryness. Finally, the solid
51 was dissolved in a minimum amount of dichloromethane to which hexanes was added to produce
52 a light yellow solid that was collected by vacuum filtration to yield pure product (0.33 g, 76%).
53
54
55
56
57
58
59
60

¹H NMR (CDCl₃, 500 MHz): δ 7.51 (dt, *J* = 1.4 Hz, *J* = 7.5 Hz, 2H), 7.44 (dd, *J* = 1.4 Hz, *J* = 7.5 Hz, 2H), 7.39 (dd, *J* = 1.5 Hz, *J* = 7.4 Hz, 2H), 7.20 (dd, *J* = 1.4 Hz, *J* = 7.6 Hz, 2H), 7.12 (t, *J* = 7.15 Hz, 2H), 6.48 (dd, *J* = 1.4 Hz, *J* = 9.2 Hz, 2H), 5.45 (d, *J* = 6.9 Hz, 2H), 3.0 (s, 6H). ¹³C NMR (CDCl₃, 126 MHz): δ 139.59 (s), 138.44 (s), 133.70 (s), 132.26 (s), 130.48 (s), 129.88 (s), 129.62 (s), 128.45 (s), 128.31 (s), 118.90 (s), 118.79 (s), 34.59 (s). HR-ESI-MS (M⁺) *m/z* calc. for [3+Cs⁺], 501.0579, Found, 501.0574.

2,2'-bis(6-bromopyridin-2-yl)-1,1'-biphenyl, 4: In an oven-dried flask, 10 equivalents of phosphorus(V) oxybromide (1.95 g, 6.8 mmol) was added to **3** (0.25 g, 0.68 mmol) and heated to 105 °C overnight with stirring under nitrogen atmosphere. The reaction was allowed to cool to room temperature and quenched with aqueous NH₄OH until strongly basic. The resulting precipitate was collected by filtration and washed with water. Dichloromethane was used to dissolve the solid before it was washed three times with water in a separatory funnel. The organic phase was dried over anhydrous sodium sulfate and evaporated to dryness to afford a light yellow solid (0.29 g, 92%). ¹H NMR (CDCl₃, 500 MHz): δ 7.53 (m, 2H), 7.49 – 7.44 (m, 2H), 7.45 – 7.39 (m, 4H), 7.27 (dd, *J* = 0.9 Hz, *J* = 7.8 Hz, 2H), 7.20 (t, *J* = 7.7 Hz, 2H), 6.68 (dd, *J* = 0.85 Hz, *J* = 7.6, 0.9 Hz, 2H). ¹³C NMR (CDCl₃, 126 MHz): δ 158.70 (s), 141.59 (s), 139.54 (s), 138.47 (s), 137.83 (s), 131.29 (s), 130.41(s), 129.39 (s), 128.28 (s), 125.87 (s), 123.34 (s). HR-ESI-MS (M⁺) *m/z* calc. for [4+Cs⁺], 596.8578, Found, 596.8571.

2,2'-di([2,2'-bipyridin]-6-yl)-1,1'-biphenyl, 5 (bpbb): In an oven-dried flask, **4** (0.25 g, 0.50 mmol) was dissolved in anhydrous toluene to which a solution of 2-tributylstannylpyridine (0.49 g, 1.33 mmol) in anhydrous toluene was added dropwise. Then, 0.8 mol % of Pd(PPh₃)₄ (4.9 mg, 0.004 mmol) was added and the reaction mixture was refluxed for 72 hours. After it was cooled to room temperature, the solvent was removed, and purification was achieved by silica gel column chromatography eluting with 1:1:0.1 ethyl acetate:hexanes:dichloromethane to yield a white solid (0.143 g, 82%). ¹H NMR (500 MHz, CDCl₃): δ 8.58 (d, *J* = 4.8 Hz, 1H), 8.06 (d, *J* = 7.8 Hz, 1H), 7.65 – 7.57 (m, 2H), 7.53 (d, *J* = 7.4 Hz, 2H), 7.47 (t, *J* = 7.2 Hz, 1H), 7.43 – 7.24 (m, 2H), 7.25 – 7.20 (m, 1H), 6.84 (d, *J* = 7.8 Hz, 1H). ¹³C NMR spectra matched previously reported data.² HR-ESI-MS (M⁺) *m/z* calc. for [5+H⁺], 463.1923, Found, 463.1917.

5-Mn, [Mn(bpbb)(OH₂)(OTf)](OTf): In a round bottom flask, [Mn(MeCN)₂(OTf)₂]_n (47 mg, 0.11 mmol) and **5** (50 mg, 0.11 mmol) were added and subsequently dissolved in acetonitrile. After stirring under nitrogen at room temperature overnight, the reaction mixture was taken to dryness by rotary evaporation. The manganese complex was recrystallized from acetonitrile with slow diethyl ether diffusion. Crystals were collected, dried under vacuum, and exposed to air to give the compound as indicated. Yield = 94 mg (90%). Elem. Anal. calc. for C₃₄H₂₄F₆MnN₄O₇S₂: C, 48.99; H, 2.90; N, 6.72. Found: C, 49.08; H, 3.01; N, 6.67. HR-ESI-MS (M⁺) *m/z* calc. for [Mn(bpbb)(OTf)]⁺, 666.0745, Found, 666.0731.

5-Fe, [Fe(bpbb)(MeCN)(OTf)](OTf): In a round bottom flask, Fe(OTf)₂ (0.11 g, 3.1 mmol) and **5** (0.14 g, 3.1 mmol) were added and subsequently dissolved in methanol. The mixture was stirred under nitrogen at room temperature overnight. The solvent was subsequently removed by rotary evaporation, and the solid was re-dissolved in acetonitrile. Crystals were obtained by slow diffusion of diethyl ether into the concentrated solution. Yield = 93 mg (89%). Elem. Anal. calc. for C₃₆H₂₅F₆FeN₅O₆S₂·(H₂O)_{1.5}·(C₄H₁₀O)_{0.5}: C, 49.52; H, 3.61; N, 7.60. Found: C, 49.27; H, 3.57; N, 7.20. HR-ESI-MS (M⁺) *m/z* calc. for [Fe(bpbb)(OTf)]⁺, 667.0715, Found, 667.0717.

5-Co, [Co(bpbb)(MeCN)(OTf)](OTf): In a round bottom flask, Co(MeCN)₂(OTf)₂ (48 mg, 0.11 mmol) and **5** (50 mg, 0.11 mmol) were added and subsequently dissolved in acetonitrile. After stirring under nitrogen at room temperature overnight, the pink orange reaction mixture

was concentrated. Crystals of the cobalt complex were obtained by slow diethyl ether diffusion into the solution, collected, dried under vacuum. Yield = 95 mg (90%). Elem. Anal. calc. for $C_{36}H_{25}CoF_6N_5O_6S_2 \cdot (H_2O)_{1.5} \cdot (C_4H_{10}O)_{0.5}$: C, 49.36; H, 3.60; N, 7.57. Found: C, 49.14; H, 3.49; N, 7.23. HR-ESI-MS (M^+) m/z calc. for $[Co(bpbb)(OTf)]^+$, 670.0696, Found, 670.0615.

5-Ni, $[Ni(bpbb)(MeCN)(ClO_4)](ClO_4)$: **Warning:** *Perchlorate salts are potentially explosive and should be handled in small amounts with care!* In a round bottom flask, $Ni(ClO_4)_2 \cdot 6H_2O$ (40 mg, 0.11 mmol) and **5** (50 mg, 0.11 mmol) were added and subsequently dissolved in acetonitrile (10 mL). After stirring under nitrogen at room temperature overnight, the light violet reaction mixture was taken to dryness by rotary evaporation. Crystals of the resulting nickel complex were grown from acetonitrile with slow diethyl ether diffusion. Yield = 84 mg (91%). Elem. Anal. calc. for $C_{34}H_{25}Cl_2N_5NiO_8 \cdot (H_2O)_{0.5} \cdot (MeCN)_{0.5}$: C, 53.16; H, 3.51; N, 9.74. Found: C, 53.12; H, 3.50; N, 9.76. HR-ESI-MS (M^+) m/z calc. for $[Ni(bpbb)(ClO_4)]^+$, 619.0683, Found, 619.0670.

5-Zn, $[Zn(bpbb)(OTf)](OTf)$: In a round bottom flask, $Zn(OTf)_2$ (39 mg, 0.11 mmol) and **5** (50 mg, 0.11 mmol) were added and subsequently dissolved in acetonitrile. After stirring under nitrogen at room temperature overnight, the colorless reaction mixture was taken to dryness by rotary evaporation. Crystals of the resulting zinc complex were grown from acetonitrile with slow diethyl ether diffusion. Yield = 91 mg (90%). 1H NMR (CD_3CN , 500 MHz): δ 8.47 (m, 3H), 8.29 (dt, $J= 1.65, 7.9$ Hz, 1H), 8.22 (dd, $J= 1.3, 5$ Hz, 1H), 8.10 (dd, $J= 2.45, 6.5$ Hz, 1H), 7.65 (dt, $J= 1.01, 5.4$ Hz, 1H), 7.50 (d, $J= 7.6$ Hz, 1H), 7.31 (t, $J= 7.5$ Hz, 1H), 7.24 (dt, $J= 0.8, 8.4$ Hz, 1H), 6.91 (d, $J= 7.65$ Hz, 1H). Elem. Anal. calc. for $C_{34}H_{22}F_6N_4O_6S_2Zn$: C, 49.44; H, 2.68; N, 6.78. Found: C, 49.71; H, 2.81; N, 6.73. HR-ESI-MS (M^+) m/z calc. for $[Zn(bpbb)]^+$, 675.0656, Found 675.0629.

5-Fe(NCS)₂, $Fe(bpbb)(NCS)_2$: In a round bottom flask, $FeSO_4 \cdot 7H_2O$ (50 mg, 0.18 mmol) and NaSCN (29 mg, 0.39 mmol) were added in methanol. The mixture was stirred under nitrogen at room temperature. The mixture immediately formed a white precipitate. The mixture was filtered through Celite. Ligand **5** (83 mg, 0.18 mmol) was added to the colorless filtrate which turned purple immediately and was stirred overnight under nitrogen. The solvent was then removed by rotary evaporation. The resulting solid was dissolved in acetonitrile, and crystals were obtained by slow diffusion of diethyl ether into the concentrated solution. Yield = 108 mg (95%). Elem. Anal. calc. for $C_{34}H_{22}FeN_6S_2$: C, 64.36; H, 3.49; N, 13.24. Found: C, 64.62; H, 3.64; N, 13.05. HR-ESI-MS (M^+) m/z calc. for $[Fe(bpbb)(NCS)]^+$, 576.0946, Found, 576.0925.

Synthesis.

The seminal publication involving ligand **5** reported a synthesis (**Figure 1A**) with an overall yield of just 18%.² We have established an improved route to this compound as shown in **Figure 1B**. Briefly, a ruthenium-catalyzed homocoupling of 2-phenylpyridine affords precursor **1**.²¹ Next, procedures for 2,2'-bipyridine functionalization were adapted,²² beginning with the methylation of **1** to form intermediate **2** as a light yellow precipitate that is simply collected by filtration. Oxidation of **2** with potassium ferricyanide gives **3** in high yield, followed by bromination with phosphorus oxytribromide to produce **4**. Notably, compound **4** is a versatile intermediate for future substitution of electronically disparate donor moieties for ligand tunability. A palladium-catalyzed Stille coupling with 2-(tributylstannyl)pyridine gives the desired bipyridine-derivatized product **5** in 30% overall yield. We note that methylation of **1** gives a mixture of mono- and dimethylated (**2**) products. In practice, the product mixture is

carried through the next two steps and undesired compounds are removed during purification of **4**, which was found to be easiest.

Complexation of metal ions Mn(II), Fe(II), Co(II), Ni(II), and Zn(II) was performed in acetonitrile or methanol solutions by stirring **5** with the appropriate metal precursor in a 1:1 ratio at room temperature overnight. Crystals were readily obtained from concentrated acetonitrile solutions by slow diethyl ether diffusion to give pure complexes in ~90% yield. The complexes are not sensitive to air and moisture.

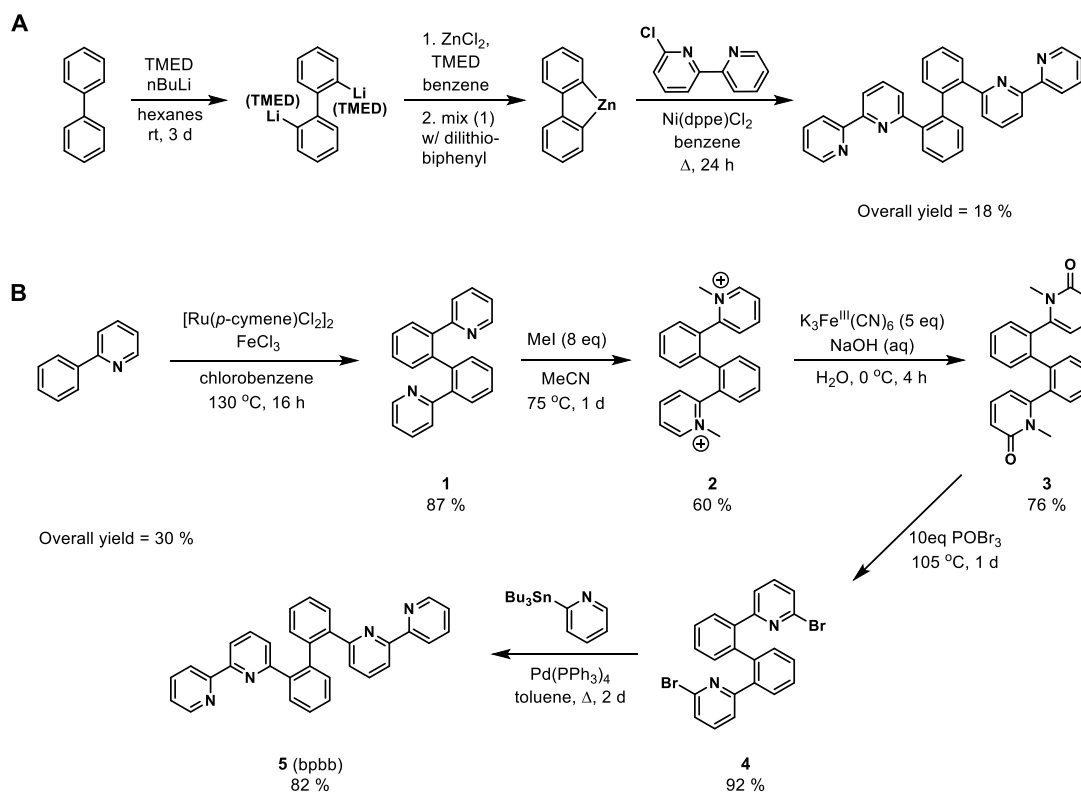


Figure 1. Synthesis of 2,2'-di([2,2'-bipyridin]-6-yl)-1,1'-biphenyl, **5**. A) Published route. B) New route to tetradentate polypyridine ligand.

X-ray Crystallography.

Solid-state structures were obtained by X-ray crystallography as shown in **Figure 2**. The complexes all crystallize in the same space group (P-1) with similar unit cell parameters as presented in **Table 1**, along with details of data collection. The biphenyl bis(bipyridine) ligand **5** (also abbreviated bpbb) is tetradentate in each complex with its metal-nitrogen bond distances ranging from 1.981 to 2.275 Å (**Table 2**). From Mn(II) to Ni(II) across the series, distorted octahedral complexes are observed. The metal-ligand bond distances found in **5-Mn**, **5-Fe**, and **5-Co** are consistent with high-spin electronic states.²³ Crystal structures of Cu(I) and Cu(II) complexes with **5** were previously reported;² selected bond distances of the Cu(II) complex are also included in **Table 2** for comparison with the M(II) complexes reported here. To clarify the coordination configuration of each metal center, coordination polyhedra of the central transition metal atoms were also derived from the crystal structure of each complex as shown in **Figure 2**.

The Cu(II) and Zn(II) compounds are five-coordinate species. Using the geometric parameter τ introduced by Addison, Reedijk, and coworkers for five-coordinate structures, the degree of distortion from ideal geometries of square pyramidal and trigonal bipyramidal can be indexed.²⁴ A value of 1 is obtained for a perfect trigonal bipyramidal geometry while τ is zero for an ideal square pyramidal geometry.²⁴ Both five-coordinate compounds possess strongly distorted trigonal bipyramidal geometries as indicated by $\tau = 0.72$ for **5-Cu'** and 0.60 for **5-Zn**.

Table 1. Crystallographic data for structures of first-row transition metal complexes supported by **5**.

	5-Mn	5-Fe	5-Co	5-Ni	5-Zn
Formula	C ₃₈ H ₃₀ F ₆ MnN ₅ O _{6.5} S ₂	C ₃₈ H ₃₀ F ₆ FeN ₅ O _{6.5} S ₂	C ₃₈ H ₃₀ CoF ₆ N ₅ O _{6.5} S ₂	C ₃₆ H ₂₈ Cl ₂ N ₆ NiO ₈	C ₃₄ H ₂₂ F ₆ N ₄ O ₆ S ₂ Zn
Formula Weight	893.73	894.64	897.72	802.25	826.04
Irradiation λ (Å), Temperature (K)	0.71073, 100(2)	0.71073, 100(2)	0.71073, 100(2)	0.71073, 100(2)	0.71073, 100(2)
Crystal System	Triclinic	Triclinic	Triclinic	Triclinic	Triclinic
Space Group	P-1	P-1	P-1	P-1	P-1
a (Å)	9.2068(3)	9.1892(2)	9.1905(5)	8.8345(3)	9.014(5)
b (Å)	13.8551(5)	13.9385(3)	13.9412(9)	13.4052(4)	13.854(5)
c (Å)	15.2249(5)	15.1654(3)	15.1233(9)	14.4981(5)	14.960(5)
α (°)	85.908(2)	86.1230(10)	86.292(2)	88.5640(10)	86.650(5)
β (°)	84.775(2)	84.0350(10)	83.904(3)	89.0040(10)	87.807(5)
γ (°)	81.762(2)	81.0590(10)	80.749(3)	88.179(2)	80.338(5)
V (Å ³)	1910.73(11)	1905.83(7)	1899.4(2)	1715.34(10)	1837.8(14)
Z	2	2	2	2	2
ρ_{calc} (g/cm ³)	1.553	1.559	1.570	1.553	1.493
μ (mm ⁻¹)	0.540	0.591	0.647	0.785	0.861
F(000)	912	914	916	824	886
Crystal Size (mm ³)	0.15 x 0.20 x 0.30	0.18 x 0.20 x 0.22	0.10 x 0.10 x 0.30	0.18 x 0.23 x 0.24	0.14 x 0.21 x 0.23
Theta range for collection (°)	1.345 to 24.406	1.35 to 25.36	1.356 to 25.458	1.52 to 25.50	1.36 to 25.38
Index ranges	-9 ≤ h ≤ 10 -16 ≤ k ≤ 16 -17 ≤ l ≤ 16	-11 ≤ h ≤ 11 -16 ≤ k ≤ 16 -18 ≤ l ≤ 18	-11 ≤ h ≤ 11 -16 ≤ k ≤ 16 -18 ≤ l ≤ 18	-10 ≤ h ≤ 10 -16 ≤ k ≤ 16 -17 ≤ l ≤ 17	-10 ≤ h ≤ 10 -16 ≤ k ≤ 16 -17 ≤ l ≤ 18
Reflectns collected	22804	49150	27618	38473	39220
Ind reflectns (R _{int})	5955 (0.0177)	6873 (0.0204)	6681 (0.0272)	6238 (0.0316)	6323 (0.0171)
Data/restr/params	5955 / 33 / 554	6873 / 2 / 550	6681 / 108 / 584	6238 / 0 / 480	6323 / 796 / 622
Final R indices [I > 2 σ (I)]	R ₁ = 0.0371, wR ₂ = 0.0861	R ₁ = 0.0270, wR ₂ = 0.0730	R ₁ = 0.0577, wR ₂ = 0.1431	R ₁ = 0.0248, wR ₂ = 0.0682	R ₁ = 0.0414, wR ₂ = 0.1075
R indices (all data)	R ₁ = 0.0417, wR ₂ = 0.0897	R ₁ = 0.0288, wR ₂ = 0.0745	R ₁ = 0.0641, wR ₂ = 0.1464	R ₁ = 0.0252, wR ₂ = 0.0685	R ₁ = 0.0445, wR ₂ = 0.1100
GOF	1.090	0.949	1.159	1.029	1.131
Largest diff. peak and hole (e Å ⁻³)	0.728 and -0.348	0.559 and -0.352	1.012 and -0.395	0.327 and -0.440	1.169 and -0.783

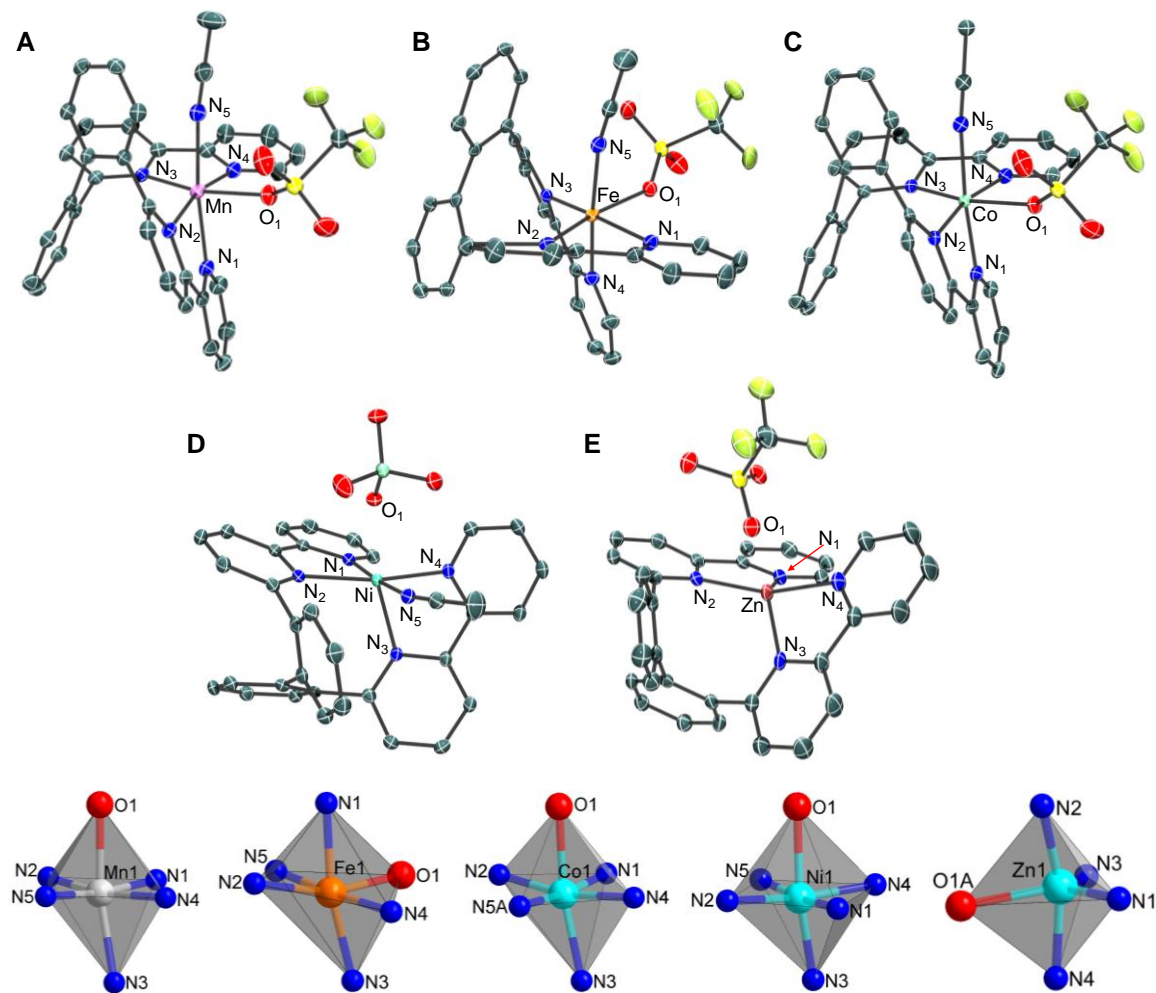


Figure 2. ORTEP diagrams of cations in **5-Mn** (A), **5-Fe** (B), **5-Co** (C), **5-Ni** (D) and **5-Zn** (E) with thermal ellipsoids rendered at the 50% probability level. Hydrogen atoms have been omitted for clarity. (Bottom) Coordination polyhedra constructed from the donor atoms that constitute the immediate coordination sphere around each transition metal ion.

Table 2. Selected bond distances of first-row metal complexes supported by **5**.

Bond Distance	Coordination Environment ^a					
	5-Mn	5-Fe	5-Co	5-Ni	5-Cu' ^b	5-Zn
M-N₁	2.238(2)	2.1748(13)	2.096(4)	2.0406(13)	1.981	2.060(2)
M-N₂	2.235(2)	2.2081(13)	2.157(4)	2.1366(13)	2.205	2.112(2)
M-N₃	2.275(2)	2.1967(13)	2.172(4)	2.1339(12)	2.037	2.086(2)
M-N₄	2.238(2)	2.1495(13)	2.131(4)	2.0622(13)	2.060	2.091(2)
M-N_{avg}	2.247	2.182	2.139	2.093	2.071	2.087
M-L	2.227(2) L = MeCN	2.1609(14) L = MeCN	2.134(8) L = MeCN	2.0585(14) L = MeCN	2.305 L = Cl	-
M-O^c	2.2001(17)	2.1491(11)	2.181(3)	2.2208(11)	-	2.21(2)
Dihedral Angle^d	121.4°	118.9°	117.0°	108.4°	119.4°	109.4°

a. All bond distances are reported in Angstroms (Å); *b.* From ref. 2 where **5-Cu'** is [Cu(bpbb)Cl](ClO₄)·MeCN; *c.* Bound oxygen donor of coordinated oxyanion, triflate or perchlorate; *d.* Dihedral angle of biphenyl backbone.

Ligated acetonitrile and an oxyanion complete the primary coordination sphere of the 6-coordinate Mn, Fe, Co, and Ni complexes. Analogous to observations reported of first-row metals supported by a pentadentate polypyridyl ligand,²³ M-N bond distances involving **5** decrease from left to right across the row in the octahedral complexes as expected from the periodic trend for effective ionic radii.²⁵ This trend is shown graphically in **Figure 3**. It is worth noting that the dihedral angle of the biphenyl backbone also decreases as the size of the metal ion becomes smaller in the 6-coordinate complexes. Although composed entirely of interconnected aromatic rings, the global flexibility in torsion angles enables **5** to accommodate metals of different size.

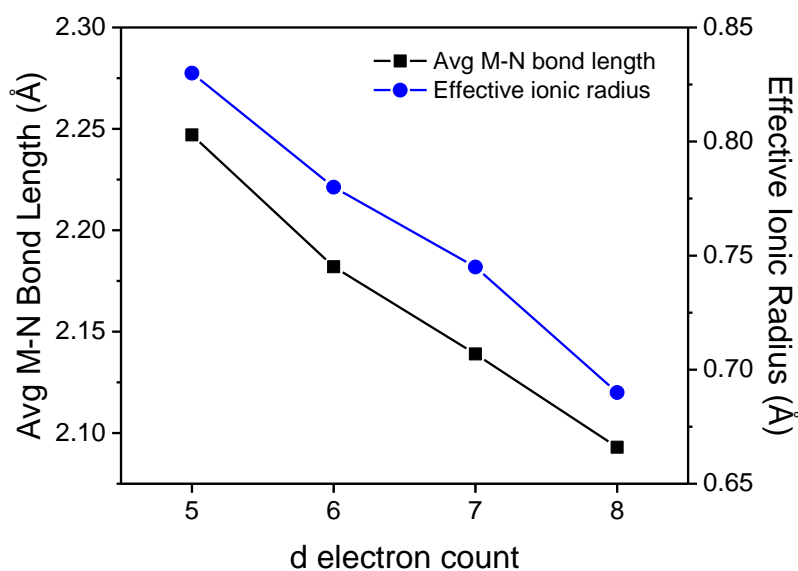


Figure 3. Plot of average metal-nitrogen bond length (Å) involving **5** and the effective ionic radius (Å) as a function of d electron count for the six-coordinate metals (**5-Mn**, **5-Fe**, **5-Co**, and **5-Ni**).

A comparison of bond distances of the pyridine donors adjacent to the biphenyl (M-N₂, M-N₃) versus the distal pyridine donors of each bipyridine unit (M-N₁, M-N₄) reveals that, in

1
2
3 general, the former have longer bond distances than the latter, indicating that the interior donors
4 are more constrained by the demands of the ligand and bind less strongly to the metal center. The
5 impact of the biphenyl bridge on the bipyridine (bpy) coordination chemistry of these complexes
6 was assessed further by comparison to relevant metal bis(bipyridine) complexes from the
7 literature. Tables S1-S6 of the Supplementary Information are grouped by each metal from
8 Mn(II) to Zn(II) and contain the metal-ligand bond distances of selected compounds, their
9 associated references, and CCDC deposition numbers.

10
11 As typically found for d^5 manganese compounds, **5-Mn** and the Mn(II) complexes listed in
12 Table S1 have bond distances that are consistent with high-spin electronic states. Interestingly,
13 the average Mn-N (bpy) bond distance observed in **5-Mn** is shorter (by ~ 0.01 to 0.02 Å) than
14 that of the related Mn(II) ions comprised of two unsubstituted 2,2'-bipyridine ligands and
15 carrying an overall charge of +1.²⁶⁻³⁰ This result is in contrast to the remaining complexes
16 supported by ligand **5** which tend to have longer M-N (bpy) bond distances relative to the
17 unsubstituted 2,2'-bipyridine donors. Given the collective preference for the high-spin electron
18 configuration, the relatively shorter M-N (bpy) bond distances observed in **5-Mn** suggests that **5**
19 is suitably matched to Mn(II), which has the largest effective ionic radius of the M(II) ions
20 investigated here, allowing stronger metal-ligand bonding interactions.

21
22 Only a limited comparison of **5-Fe** was possible with iron(II) bis(bipyridine) complexes.^{31,32}
23 Indeed, $[\text{Fe}(\text{bpy})_2\text{L}_2]^{n+}$ complexes (where L is a labile monodentate ligand) are very rare due to
24 formation of the thermodynamically favored d^6 spin-paired $[\text{Fe}(\text{bpy})_3]^{2+}$ complex.^{31,32} However,
25 crystal structures with mononuclear $\text{Fe}(\text{bpy})_2$ cores were found with anionic donors Cl^- , CN^- ,
26 and NCS^- completing the octahedral coordination spheres (Table S2).³³⁻³⁵ Despite the overall +1
27 positive charge of **5-Fe**, its average Fe-N (bpy) bond distance is longer than that of the neutral
28 compounds $\text{Fe}(\text{bpy})_2\text{Cl}_2$,³³ $\text{Fe}(\text{bpy})_2(\text{CN})_2$,³⁴ and $\text{Fe}(\text{bpy})_2(\text{NCS})_2$.³⁵ The longer bond lengths
29 observed with **5-Fe** are consistent with a high-spin electronic state and highlight the weaker
30 ligand field afforded by the rigid biphenyl-based ligand **5**. In addition, a strong temperature
31 dependence was reported for $\text{Fe}(\text{bpy})_2(\text{NCS})_2$ in solid-state structures determined at 110 and 298
32 K, which have average Fe-N (bpy) bond lengths of 1.967 and 2.174 Å, respectively, indicating a
33 change from low-spin (110 K) to high-spin (298 K).³⁵ This behavior is not observed with **5-Fe**,
34 which has an average Fe-N (bpy) bond length of 2.183 Å in the solid-state at 100 K.

35
36 Crystal structures of selected cobalt(II) complexes were also compared with **5-Co** (Table S3).
37 Again, the average cobalt-pyridine bond distance of **5-Co** (2.139 Å) was found to be longer
38 relative to other monocationic Co(II) ions,^{36,37} reflecting the structural constraints of the
39 tetradentate ligand. Nearly equivalent average Co-N (bpy) bond distances were observed
40 between **5-Co** and neutral $\text{Co}(\text{bpy})_2\text{Cl}_2$ (2.142 Å),³⁸ which are ~ 0.08 Å longer than that of
41 $[\text{Co}(\text{bpy})_2(\text{OH}_2)_2]^{2+}$ as expected on the basis of overall charge.³⁹ Similar observations were made
42 for **5-Ni** with respect to relevant octahedral nickel(II) compounds featuring two unsubstituted
43 2,2'-bipyridine donors.⁴⁰⁻⁴⁴ As summarized in Table S4, average Ni-N (bpy) bond lengths ranged
44 from 2.059 Å for $[\text{Ni}(\text{bpy})_2(\text{OH}_2)(\text{ONO}_2)]^+$ to 2.091 Å for $\text{Ni}(\text{bpy})_2\text{Cl}_2$, while the average nickel-
45 pyridine bond distance for **5-Ni** was 2.094 Å.

46
47 Next, the five-coordinate copper(II) and zinc(II) complexes were compared to related
48 bis(bipyridine) compounds (Table S5).⁴⁵⁻⁴⁷ Copper compound (**5-Cu'**) bearing **5** and a chloro
49 ligand has an average Cu-N (bpy) bond distance of 2.071 Å.² Consistent with the bridled
50 coordination of **5** noted above, this average bond distance is longer by ~ 0.02 to 0.03 Å relative to
51 the average Cu-N (bpy) bond distances found in crystal structures of several $[\text{Cu}(\text{bpy})_2\text{Cl}]^+$
52 salts.⁴⁵⁻⁴⁷ In the same vein, **5-Zn**, ligated by the biphenyl-based polypyridine and a triflate donor,
53
54
55
56
57
58
59
60

has an average zinc-pyridine bond distance of 2.088 Å which is longer than that of both [Zn(bpy)₂Cl]⁺ and [Zn(bpy)₂(OH₂)]²⁺ (Table S6).^{48,49} Together these results indicate that the biphenyl bridge restrains bipyridine coordination to mid-to-late first-row metal centers.

Electrochemistry.

Cyclic voltammetry was conducted in anhydrous acetonitrile with the title compounds (**Figure 4**). Multiple redox processes were observed in the cyclic voltammograms (CVs) over a wide potential range (> 3 V); $E_{1/2}$ values and peak potentials for the irreversible redox features are summarized in **Table 3**. All potentials are reported in volts versus the ferrocenium/ferrocene couple (V vs Fc⁺⁰). Irreversible to quasi-reversible metal-based oxidations occur at 0.67 V (**5-Mn**), 0.95 V (**5-Fe**), 0.74 V (**5-Co**), each of which is a M^{III/II} process, and at 0.09 V (**5-Cu**) which we assign to a Cu^{II/I} couple. Similar oxidations were not observed with **5-Ni** and **5-Zn**. As expected, **5-Zn** is electrochemically silent at potentials positive of -1.4 V. The zinc complex, featuring a redox-inactive metal center, is useful in identifying ligand-based redox events and has redox couples at -1.47, -1.58, and -2.17, followed by an irreversible reduction at -2.45 V. Consistent with previous observations,² **5-Cu** exhibits two ligand-based reductions at -2.07 and -2.26 V. Upon scanning positive, a sharp return oxidation is observed at -0.71 V, which is likely due to adsorption on the electrode surface given the reversible behavior previously reported with this compound in acetonitrile using Bu₄NClO₄ as the supporting electrolyte.² Compound **5-Ni** has three reversible redox processes at -1.03, -1.57, and -2.38 V that are tentatively assigned to Ni^{II/I} and Ni^{I/0} metal-based couples followed by a ligand-localized reduction, respectively. For **5-Co**, an irreversible feature at -1.03 V is assigned to a Co^{II/I} reduction with two reversible couples at -1.69 and -1.96 V occurring that are likely ligand centered. Similarities in the CVs of **5-Fe** and **5-Mn** are apparent. Each complex has a two-electron reduction at -1.53 V (**5-Fe**) and -1.71 V (**5-Mn**), which are at similar potentials to the initial overlapping one-electron reductions of **5-Zn**. On this basis, we assign these events as ligand-based reductions and the most negative waves to M^{II/I} couples.

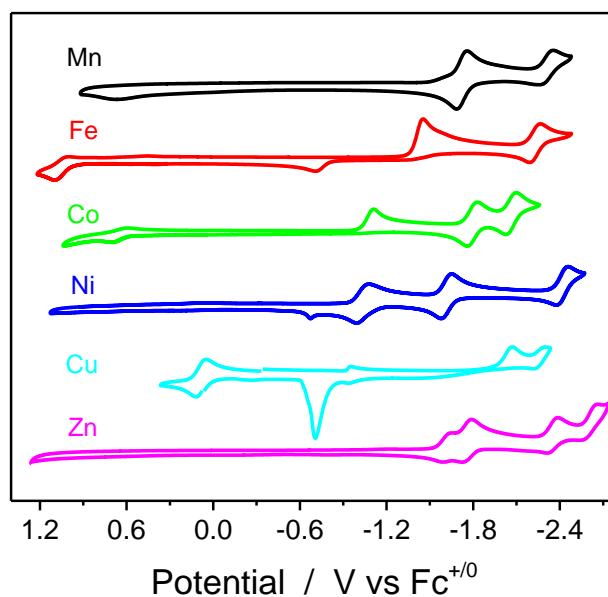


Figure 4. CVs of **5-Mn**, **5-Fe**, **5-Co**, **5-Ni**, **5-Cu**, and **5-Zn** (at 1 mM concentrations) in anhydrous acetonitrile / 0.1 M Bu₄NPF₆ solutions using a glassy carbon disk electrode, $\nu = 100$ mV/s.

Table 3. Redox properties of each complex in acetonitrile with 0.1 M Bu₄NPF₆, $\nu = 100$ mV/s.

Complex	Redox Potentials (V vs Fc ⁺⁰)				
5-Mn	0.67 ^b	-1.71	-2.30	-	-
5-Fe	0.95 ^b	-1.53 ^c	-2.30	-	-
5-Co	0.74	-1.03 ^c	-1.69	-1.96	-
5-Ni	-	-1.03	-1.57	-2.38	-
5-Cu^a	0.09	-0.71 ^b	-2.07 ^c	-2.26 ^c	-
5-Zn	-	-1.47	-1.58	-2.17	-2.45 ^c

a. **5-Cu** is [Cu(bpbb)](ClO₄)₂·MeCN·H₂O as reported in ref. 2; b. Irreversible ($E_{p,a}$); c. Irreversible ($E_{p,c}$).

To assess the influence of the biphenyl backbone on redox potentials, the electrochemical data summarized in **Table 3** was compared to related first-row metal bis- and tris-bipyridine complexes (Table S7).^{36,50-58} Here, bipyridine-based reductions were generally found from approximately -1.3 to -2.3 V vs Fc⁺⁰. Interestingly, metal-based redox couples of the complexes supported by **5** are typically more positive than those of the corresponding [M(bpy)₃]²⁺ complexes, with the exception of **5-Mn**. The processes assigned to the Fe^{III/II} couples of **5-Fe** and [Fe(bpy)₃]²⁺ occur at 0.95 and 0.69 V, respectively,⁵¹ whereas the Mn^{III/II} couples of **5-Mn** and [Mn(bpy)₃]²⁺ appear at 0.67 and 0.93 V, respectively.⁵⁰ Likewise, the Cu^{II/I} couple of **5-Cu** is observed at 0.09 V, or nearly 600 mV more positive than for [Cu(bpy)₃]²⁺.⁵⁷ These metal-based redox potentials are consistent with the observed metal-pyridine bond distances. Stronger Lewis acid-base bonding interactions are observed in **5-Mn** compared to related Mn(II) compounds, which results in greater electron density at the metal and a cathodic shift of the Mn^{III/II} couple. However, weaker bonds to each metal center are present for the remaining compounds relative to their [M(bpy)₃]²⁺ counterparts, which give rise to anodic shifts in the metal-based redox couples.

UV-visible Spectroscopy.

UV-visible spectra of the compounds in acetonitrile are shown in **Figure 5**; associated absorption maxima and molar extinction coefficients are presented in **Table 4**. An intense π -to- π^* transition at around 310 nm (~ 22000 M⁻¹cm⁻¹) is observed for all five metal complexes. Given the high-spin electronic states afforded by the constrained biphenyl bis(bipyridine) ligand, the complexes have little-to-no absorbance in the visible region. The iron complex **5-Fe** has a weak absorption band at 410 nm (660 M⁻¹cm⁻¹) that is ascribed to a metal-to-ligand charge transfer (MLCT) transition. Broad, low-intensity bands assigned to Laporte-forbidden d-d transitions are observed at 815 nm (**5-Fe**), 482 nm (**5-Co**), and 550 and 923 nm (**5-Ni**) consistent with the solid-state structures and distorted octahedral compounds in solution. Likewise, two broad bands at 677 and 960 nm are characteristic of **5-Cu**.

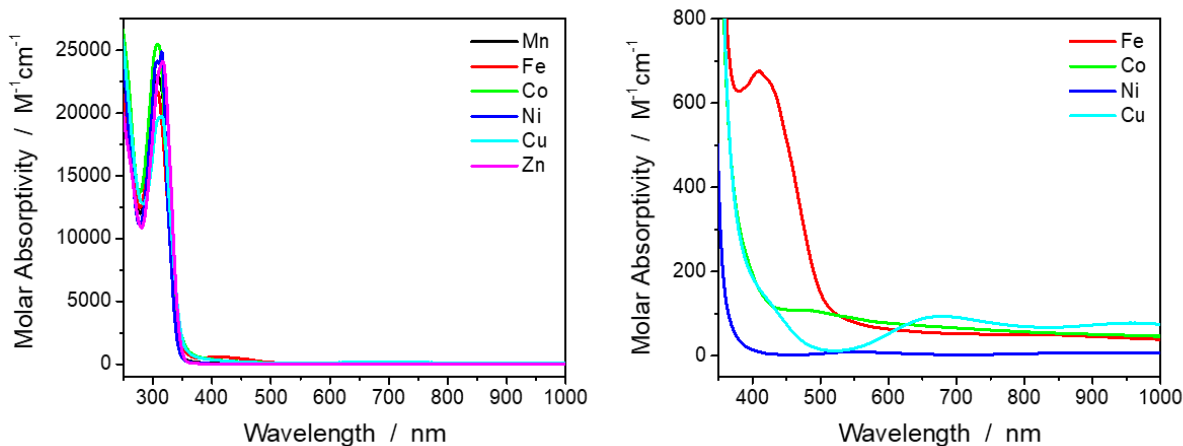


Figure 5. UV-visible spectra of Mn(II), Fe(II), Co(II), Ni(II), Cu(II), and Zn(II) complexes with ligand **5** in acetonitrile.

Table 4. UV-vis spectral properties and solution magnetic susceptibility of metal complexes bearing **5**.

5-Mn	5-Fe	5-Co	5-Ni	5-Cu	5-Zn
UV-Vis					
308 (22827)	307 (22100) 410 (660) 815 (50)	308 (25100) 482 (110)	307 (23800) 550 (10) 923 (10)	315 (19000) 677 (100) 960 (100)	317 (23500)
μ_{eff} at 298 K (μ_{B})					
5.9	5.2	4.5	2.7	1.5	-

Magnetism.

The Evans method was used to determine solution magnetic susceptibilities across the series as summarized in **Table 4**. The experimental magnetic moments are close to the theoretical values expected for high-spin electronic states and/or the d^n electron configuration of each M(II) ion, for example, as in d^9 Cu(II) which will have one unpaired electron regardless of geometry or spin state. The deviation in the measured value ($4.5 \mu_{\text{B}}$) for **5-Co** from the anticipated theoretical spin-only magnetic moment ($3.87 \mu_{\text{B}}$) is common of cobalt complexes, including a previously reported high-spin Co(II) polypyridyl complex,²³ and indicative of an overall magnetic moment with significant orbital contribution.⁵⁹

Intrigued by the work of Petzold and coworkers who have developed iron(II) compounds supported by hexadentate and dinucleating biphenyl-based N-donor ligands that exhibit spin crossover behavior,⁵ we prepared a bis(thiocyanato) derivative **5-Fe(NCS)₂**, in addition to **5-Fe**. Their temperature-dependent magnetic behavior was investigated by solid-state SQUID magnetometry. For compounds **5-Fe** and **5-Fe(NCS)₂**, the plots of DC susceptibility vs. temperature exhibited room temperature $\chi_{\text{m}}T$ values of $3.98 \text{ emu}\cdot\text{K/mol}$ and $3.76 \text{ emu}\cdot\text{K/mol}$ (indicative of electron g -factors greater than 2.00), which steadily decreased to final $\chi_{\text{m}}T$ values of $2.70 \text{ emu}\cdot\text{K/mol}$ and $1.64 \text{ emu}\cdot\text{K/mol}$ respectively (**Figure 6**). Room temperature $\chi_{\text{m}}T$ values for high-spin Fe(II) complexes are generally in the range of 3 – 3.5,⁶⁰ but higher values have been reported as well.⁶¹ This steady decrease in $\chi_{\text{m}}T$ can be attributed to zero-field splitting in the

complexes and/or thermal depopulation of excited electronic states. Spin crossover behavior was not observed as the compounds maintained high-spin electron configurations over the entire temperature range, as indicated by the absence of a precipitous drop of the $\chi_m T$ values at lower temperatures.

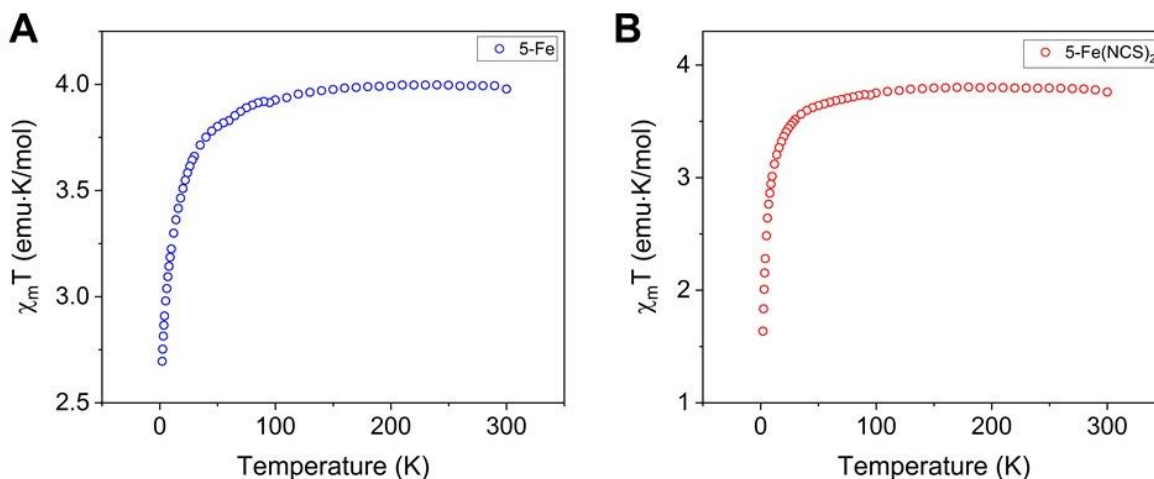


Figure 6. Temperature dependence of $\chi_m T$ for **5-Fe** (A) and **5-Fe(NCS)₂** (B).

Conclusions.

In closing, we report an improved synthesis of a rigid polyaromatic N₄-donor ligand and have greatly expanded its known coordination chemistry. Structural, electrochemical, spectroscopic, and magnetic properties of a series of mid-to-late first-row transition metal complexes supported by the tetradentate polypyridine scaffold have been investigated. From X-ray crystallography, the ligand field around each metal ion is noticeably constrained by the limited flexibility (confined to rotation about the single bonds connecting each aromatic unit) afforded by the biphenyl backbone. High spin electronic states, based in part on the metal-ligand bond lengths, and distorted octahedral geometries are observed for the Mn(II), Fe(II), and Co(II) complexes. Distorted trigonal bipyramidal geometries are found in solid-state structures of the Cu(II) and Zn(II) derivatives. Indeed, the optical spectra, solution magnetic susceptibility measurements, and temperature-dependent SQUID magnetometry data are consistent in both the solid-state and solution analyses, confirming the structural integrity of the dissolved complexes remains intact.

Notably, **5-Fe** represents a rare example of an iron bis(bipyridine) complex possessing two labile monodentate ligands. Synthetic routes to [Fe(bpy)₂L₂]ⁿ⁺ complexes are elusive due to the favored formation of the tris(bpy) complex, which is a consequence of a change from high spin to low spin between [Fe(bpy)₂L₂]ⁿ⁺ to the more stable spin-paired [Fe(bpy)₃]²⁺ ion.^{31,32} We hypothesize that the biphenyl-linked bis(bipyridine) ligand may prevent this spin change and negate the thermodynamic driving force that would otherwise favor the tris(bpy) derivative. Spin crossover behavior was not observed in the iron(II) compounds **5-Fe** and **5-Fe(NCS)₂**. These results indicate that **5** weakens the ligand field strength around iron and, due to its limited flexibility, may be less accommodating to the changes in metal-ligand bond distances that accompany a spin transition from high-to-low.

Conflicts of Interest.

There are no conflicts to declare.

Acknowledgements.

Acknowledgment is made to the donors of The American Chemical Society Petroleum Research Fund for support of this research (58707-DNI3). We also acknowledge seed grant funding from the National Science Foundation (OIA-1539035) and start-up support from the University of Mississippi.

References.

1. (a) T. J. Collins, *Acc. Chem. Res.*, 1994, **27**, 279-285; (b) P. Comba, *Coord. Chem. Rev.*, 1999, **182**, 343-371; (c) R. D. Hancock, *Chem. Soc. Rev.*, 2013, **42**, 1500-1524.
2. E. Müller, C. Piguet, G. Bernardinelli and A. F. Williams, *Inorg. Chem.*, 1988, **27**, 849-855.
3. (a) O. P. Anderson, J. Becher, H. Frydendahl, L. F. Taylor and H. Toftlund, *J. Chem. Soc., Chem. Commun.*, 1986, 699-701; (b) S. Knapp, T. P. Keenan, X. Zhang, R. Fikar, J. A. Potenza and H. J. Schugar, *J. Am. Chem. Soc.*, 1990, **112**, 3452-3464; (c) E. Müller, G. Bernardinelli and J. Reedijk, *Inorg. Chem.*, 1996, **35**, 1952-1957; (d) M. R. Malachowski, M. Adams, N. Elia, A. L. Rheingold and R. S. Kelly, *J. Chem. Soc., Dalton Trans.*, 1999, 2177-2182.
4. (a) M. Réglie, C. Jorand and B. Waegell, *J. Chem. Soc., Chem. Commun.*, 1990, 1752-1755; (b) M. R. Malachowski, A. S. Kasto, M. E. Adams, A. L. Rheingold, L. N. Zakharov, L. D. Margerum and M. Greaney, *Polyhedron*, 2009, **28**, 393-397.
5. (a) H. Petzold and S. Heider, *Eur. J. Inorg. Chem.*, 2011, 1249-1254; (b) S. Heider, H. Petzold and G. Teucher, *Eur. J. Inorg. Chem.*, 2013, 2382-2388.
6. (a) M. Kettunen, C. Vedder, F. Schaper, M. Leskelä, I. Mutikainen and H.-H. Brintzinger, *Organometallics*, 2004, **23**, 3800-3807; (b) C. Vedder, F. Schaper, H.-H. Brintzinger, M. Kettunen, S. Babik and G. Fink, *Eur. J. Inorg. Chem.*, 2005, 1071-1080; (c) G. J. P. Britovsek, J. England and A. J. P. White, *Dalton Trans.*, 2006, 1399-1408; (d) T. Chen, X.-G. Liu and M. Shi, *Tetrahedron*, 2007, **63**, 4874-4880.
7. M. A. Halcrow, *Polyhedron*, 2007, **26**, 3523-3576.
8. S. O. Schmidt, S. Kisslinger, C. Würtele, S. Bonnet, S. Schindler and F. Tuzcek, *Z. Anorg. Allg. Chem.*, 2013, **639**, 2774-2778.
9. P. Gütllich, A. B. Gaspar and Y. Garcia, *Beilstein J. Org. Chem.*, 2013, **9**, 342-391.
10. (a) A. Bousseksou, G. Molnár, L. Salmon and W. Nicolazzi, *Chem. Soc. Rev.*, 2011, **40**, 3313-3335; (b) S. Brooker, *Chem. Soc. Rev.*, 2015, **44**, 2880-2892; (c) M. A. Halcrow, *Crystals*, 2016, **6**, 58.
11. E. C. Constable, G. Baum, E. Bill, R. Dyson, R. van Eldik, D. Fenske, S. Kaderli, D. Morris, A. Neubrand, M. Neuburger, D. R. Smith, K. Wieghardt, M. Zehnder and A. D. Zuberbühler, *Chem. Eur. J.*, 1999, **5**, 498-508.
12. E. D. McKenzie, *Coord. Chem. Rev.*, 1971, **6**, 187-216.
13. D. Onggo and H. A. Goodwin, *Aust. J. Chem.*, 1991, **44**, 1539-1551.
14. (a) L. Chen, A. Khadivi, M. Singh and J. W. Jurss, *Inorg. Chem. Front.*, 2017, **4**, 1649-1653; (b) X. Su, K. M. McCardle, J. A. Panetier and J. W. Jurss, *Chem. Commun.*, 2018, **54**, 3351-3354; (c) W. Yang, S. Sinha Roy, W. C. Pitts, R. Nelson, F. R. Fronczek and J. W. Jurss, *Inorg. Chem.*, 2018, **57**, 9564-9575.

15. (a) D. F. Evans, *J. Chem. Soc.*, 1959, 2003-2005; (b) G. A. Bain and J. F. Berry, *J. Chem. Ed.*, 2008, **85**, 532-536.
16. APEX2, v. 2009; Bruker Analytical X-Ray Systems, Inc: Madison, WI, 2009.
17. G. M. Sheldrick, SADABS, Version 2.03; Bruker Analytical X-ray Systems, Inc: Madison, WI, 2000.
18. (a) G. M. Sheldrick, *Acta Crystallogr., Sect. A: Found. Crystallogr.*, 1990, **46**, 467-473; (b) G. M. Sheldrick, *Acta Crystallogr., Sect. A: Found. Crystallogr.*, 2008, **64**, 112-122; (c) G. M. Sheldrick, SHELXL-2014/7: Program for crystal structure determination, University of Göttingen: Göttingen, Germany, 2014.
19. (a) A. L. Spek, PLATON - A Multipurpose Crystallographic Tool, Utrecht University, Utrecht, The Netherlands, 2007; (b) A. L. Spek, PLATON SQUEEZE: A tool for the calculation of the disordered solvent contribution to the calculated structure factors. *Acta Crystallogr., Sect. C: Struct. Chem.*, 2015, **71**, 9-18.
20. H. Putz and K. Bradenburg, *Diamond - Crystal and Molecular Structure Visualization*, Crystal Impact: GbR, Kreuzherrenstr. 102, 53227 Bonn, Germany, <http://www.crystalimpact.com/diamond>.
21. X. Guo, G. Deng, C.-J. Li, *Adv. Synth. Catal.*, 2009, **351**, 2071-2074.
22. M. Böttger, B. Wiegmann, S. Schaumburg, P. G. Jones, W. Kowalsky and H.-H. Johannes, *Beilstein J. Org. Chem.*, 2012, **8**, 1037-1047.
23. R. J. M. Klein Gebbink, R. T. Jonas, C. R. Goldsmith and T. D. P. Stack, *Inorg. Chem.*, 2002, **41**, 4633-4641.
24. A. W. Addison, T. N. Rao, J. Reedijk, J. van Rijn and G. C. Verschoor, *J. Chem. Soc., Dalton Trans.*, 1984, 1349-1356.
25. R. D. Shannon, *Acta Crystallogr.*, 1976, **A32**, 751-767.
26. N. Palanisami and R. Murugavel, *Inorg. Chim. Acta*, 2011, **365**, 430-438.
27. K. B. Dillon, C. Bilton, J. A. K. Howard, V. J. Hoy, R. M. K. Deng and D. T. Sethatho, *Acta Crystallogr., Sect. C: Cryst. Struct. Commun.*, 1999, **C55**, 330-332.
28. M. Shao, Z.-X. Miao and M.-X. Li, *Acta Crystallogr., Sect. E: Struct. Rep. Online*, 2006, **E62**, m2575-m2577.
29. G. Fernández, M. Corbella, M. Alfonso, H. Stoeckli-Evans and I. Castro, *Inorg. Chem.*, 2004, **43**, 6684-6698.
30. X.-M. Chen, K.-L. Shi, T. C. W. Mak and B.-S. Luo, *Acta Crystallogr., Sect. C: Cryst. Struct. Commun.*, 1995, **C51**, 358-361.
31. H. Irving and D. H. Mellor, *J. Chem. Soc.*, 1962, 5222-5237.
32. M.-N. Collomb, A. Deronzier, K. Gorgy and J.-C. Leprêtre, *New J. Chem.*, 2000, **24**, 455-461.
33. S. Parsons, R. Winpenney and P. A. Wood, *CCDC 248214: Experimental Crystal Structure Determination*, 2014, DOI: 10.5517/cc8b8xr.
34. Y. Wang, X. Ma, S. Hu, Y. Wen, Z. Xue, X. Zhu, X. Zhang, T. Sheng and X. Wu, *Dalton Trans.*, 2014, **43**, 17453-17462.
35. M. Konno and M. Mikami-Kido, *Bull. Chem. Soc. Jpn.*, 1991, **64**, 339-345.
36. S.-P. Luo, L.-Z. Tang and S.-Z. Zhan, *Inorg. Chem. Commun.*, 2017, **86**, 276-280.
37. S. Gao, J.-W. Liu, L.-H. Huo and H. Zhao, *Acta Crystallogr., Sect. E: Struct. Rep. Online*, 2004, **E60**, m1202-m1204.
38. V. Ciornea, L. Mingalieva, J.-P. Costes, G. Novitchi, I. Filippova, R. T. Galeev, S. Shova, V. K. Voronkova and A. Gulea, *Inorg. Chim. Acta*, 2008, **361**, 1947-1957.

39. K. A. Kumar, M. Amuthaselvi and A. Dayalan, *Acta Crystallogr., Sect. E: Struct. Rep. Online*, 2011, **E67**, m468.
40. B.-S. Zhang, Z.-X. Liu, L.-H. Liu, T. Pan and S.-F. Ye, *Acta Crystallogr., Sect. E: Struct. Rep. Online*, 2009, **E65**, m48.
41. M. Garai, D. Dey, H. R. Yadav, A. R. Choudhury, N. Kole and B. Biswas, *Polyhedron*, 2017, **129**, 114-122.
42. D. J. Chesnut, R. C. Haushalter and J. Zubieta, *Inorg. Chim. Acta*, 1999, **292**, 41-51.
43. Y. Rodríguez-Martín, J. González-Platas and C. Ruiz-Pérez, *Acta Crystallogr., Sect. C*, 1999, **C55**, 1087-1090.
44. B. Hipler, M. Döring, C. Dubs, H. Görls, T. Hübler and E. Uhlig, *Z. Anorg. Allg. Chem.*, 1998, **624**, 1329-1335.
45. M. A. Sharif, M. Tabatabaee, V. Beik and H. R. Khavasi, *CCDC 749881: Experimental Crystal Structure Determination*, 2014, DOI: 10.5517/cct59qz.
46. A. Jayamani, N. Sengottuvelan, S. K. Kang and Y.-I. Kim, *Polyhedron*, 2015, **98**, 203-216.
47. P. Nagle, E. O'Sullivan, B. J. Hathaway and E. Müller, *J. Chem. Soc., Dalton Trans.*, 1990, **0**, 3399-3406.
48. J.-C. Yao, F.-J. Yao, J.-B. Guo, W. Huang, S.-H. Gou, *CCDC 271110: Experimental Crystal Structure Determination*, 2014, DOI: 10.5517/cc933hz.
49. G. Singh, I. P. S. Kapoor, D. Kumar, U. P. Singh and N. Goel, *Inorg. Chim. Acta*, 2009, **362**, 4091-4098.
50. S. A. Richert, P. K. S. Tsang and D. T. Sawyer, *Inorg. Chem.*, 1989, **28**, 2471-2475.
51. J. P. F. Rebolledo-Chávez, M. Cruz-Ramírez, R. Patakfalvi, F. J. Tenorio Rangel and L. Ortiz-Frade, *Electrochimica Acta*, 2017, **247**, 241-251.
52. M.-N. Collomb, A. Deronzier, K. Gorgy and J.-C. Leprêtre, *New J. Chem.*, 2000, **24**, 455.
53. M. A. W. Lawrence and A. A. Holder, *Inorg. Chim. Acta*, 2016, **441**, 157.
54. R. Prasad and D. B. Scaife, *J. Electroanal. Chem.*, 1977, **84**, 373-386.
55. P. N. Bartlett and V. Eastwick-Field, *Electrochimica Acta*, 1993, **38**, 2515-2523.
56. O. S. Fomina, Y. A. Kislitsyn, V. M. Babaev, I. K. Rizvanov, O. G. Sinyashin, J. W. Heinicke and D. G. Yakhvarov, *Russian J. Electrochem.*, 2015, **51**, 1069-1078.
57. R. R. Ruminski, *Inorg. Chim. Acta*, 1985, **103**, 159-161.
58. R. J. Crutchley, R. Hynes and E. J. Gabe, *Inorg. Chem.*, 1990, **29**, 4921-4928.
59. F. A. Cotton and G. Wilkinson, *Advanced Inorganic Chemistry*, 5th edition; Wiley-Interscience: New York, 1988.
60. S. Kisslinger, H. Kelm, S. Zheng, A. Beitat, C. Würtele, R. Wortmann, S. Bonnet, S. Herres-Pawlis, H.-J. Krüger and S. Schindler, *Z. Anorg. Allg. Chem.*, 2012, **638**, 2069-2077.
61. A. Kimura and T. Ishida, *Inorganics*, 2017, **5**, 52-63.

Table of Contents Entry

